Polarity-manipulation based on nanoscale structural transformation on strained 2D MgO

2014 J. Phys. D: Appl. Phys. 47 105303

(http://iopscience.iop.org/0022-3727/47/10/105303)

IOP Publishing Journal of Physics D: Applied Physics
J. Phys. D: Appl. Phys. **47** (2014) 105303 (8pp) doi:10.1088/0022-3727/47/10/105303

Polarity-manipulation based on nanoscale structural transformation on strained 2D MgO

Zhanglong Liu, Xiang He, Zengxia Mei, Huili Liang, Lin Gu, Xiaofeng Duan and Xiaolong Du

Beijing National Laboratory for Condensed Matter Physics, Institute of Physics, Chinese Academy of Sciences, Beijing 100190, People's Republic of China

E-mail: zxmei@aphy.iphy.ac.cn

Received 28 June 2013, revised 7 November 2013
Accepted for publication 13 January 2014
Published 19 February 2014

Abstract

Strain induced nanoscale structural transformation is demonstrated in this paper to have the ability of triggering polarity flipping in a wide bandgap system of $Mg_xZn_{1-x}O/MgO/Al_2O_3$. Relaxation dynamics of semiconductor components under large compressive pressures up to 13.7 GPa were studied by a combination of theoretical analysis and experimental characterizations including *in situ* reflection high-energy electron diffraction and high-resolution transmission electron microscopy. The gigantic force between MgZnO and ultrathin-MgO/Al_2O_3 delayed the structural transformation of MgZnO from six-fold cubic to four-fold wurtzite into the second monolayer, and consequently flipped the polarity of the film deposited on relaxed MgO. Additionally, dislocation-induced strain relaxation was suggested to happen around 1 nm thick cubic MgO grown on Al_2O_3, instead of the previous well-accepted concept that wurtzite structures can be inherited from the oxygen sub-lattice of sapphire substrates below the critical thickness. Finally, the structural transformation method employing an ultrathin-MgO interfacial layer was demonstrated to be a suitable technique for accommodating the large lattice mismatch comparing with the dislocation-relaxation mechanism achieving a UV photodetector with four orders of rejection ratio of the UV-to-visible photoresponse.

Keywords: MgZnO, ZnO, polarity, UV-detector, structural transformation

(Some figures may appear in colour only in the online journal)

The persistent interest in manipulating the polarity of polar materials probably arises from its great influence on the bulk electric field distribution, interface/surface energetic states, chemical properties, and finally device performance [1]. It is especially significant for oxide semiconductors owing to their abundance on Earth and increasingly massive research/industrial applications. For example, delicate control of the polarity inside a zinc oxide semiconductor can be utilized to enhance the energy harvesting ability of ZnO-based nano-generators [2], to control chemical environments for biosensors [3], and to achieve two-dimensional electron gas (2DEG) in MgZnO/ZnO interfaces [4]. As a result, any technique or method that can be used to engineer the single polarity in these oxide materials is of great interest and importance. Considering the close connections between crystal structures and polarities [5, 6], high-pressure techniques are good candidates for this kind of study due to the versatile abilities in alternating material structures. They have contributed a lot to scientific explorations and discoveries across various research disciplines [7–10]. However, investigations on high-pressure induced metastable crystal structures and polarity-related issues are not straight forward and the phenomena are usually superimposed on others. In this case, it becomes much more difficult to achieve an unambiguous conclusion of the direct connections between pressure and polarity alternation mechanism, especially for the compound semiconductor materials which are fabricated by complex processes, molecular beam epitaxy (MBE) and metal organic

chemical vapour deposition (MOCVD) for instance. Possible reasons may be the infinite number of growth conditions which complicate the problem. In these processes, it is necessary to adopt suitable buffer (interfacial) layers to modify the complex substrate surface structures and realize a unipolar epitaxial film with high crystal quality. The interface between buffer layer and epilayer plays a key role in the polarity selection inside the epilayer. In some cases, the buffer layers are several nanometres thick, and in an unrelaxed and highly strained condition. Achieving well-defined atomic-resolution images and a deep understanding of these interface structures becomes the major target for a clear elucidation of the connections between crystal structures and polarities, especially for the nanometre-scale interfacial structures under high-pressure states.

It has been well established in experiments that the thickness and crystalline structures of the MgO interfacial layer in a $Mg_xZn_{1-x}O$/MgO/Al_2O_3 system could determine the polarity of the wide bandgap $Mg_xZn_{1-x}O$ semiconductor [11]. An empirical theory of polarity flipping from Zn- to O-polarity inside $Mg_xZn_{1-x}O$ was postulated and well accepted, which assumes that the structural change of MgO from cubic into hexagonal (wurtzite) symmetry happens and decides the polarities when the thickness decreases less than 2 nm [11]. This explanation of the polarity selection behaviour and assumption of wurtzite-MgO phase were accepted broadly, partly because this nanometre-thick atomic-flat MgO layer was revealed to be so perfect that it should not be (1 1 1) polar planes of rock-salt cubic MgO which was found bearing significant roughness. Additionally, the conclusion of cubic-MgO/wurtzite-MgO transition on Al_2O_3 was made from Martinez-Boubeta *et al* [12] by using a magnetron sputtering growth technique and transmission electron microscopy (TEM) structural characterization. However, a poor crystalline quality of MgO and an ambiguous TEM image made the conclusion questionable. This argument became vulnerable when the wurtzite phase was found to be an unfavourable high-energy state for MgO under compressive strain [13]. According to previous energetic-structural calculations [13–15], rock-salt MgO occupies the lowest energy state in equilibrium comparing with other possible crystalline structures under external compressive pressure and thus becomes the only candidate of the structures of MgO on Al_2O_3. Therefore, the mechanisms were still uncertain and the major issue focused on the clarification of the MgO structure under high pressures and its effect on the polarity inheriting choice. We have revealed that nanometre-thick MgO has a clearly unrelaxed cubic structure with big compressive strains [14], not the wurtzite phase as claimed in previous reports. Regarding the polarity selection mechanism, we postulated before that maybe it was the alloy effect that caused the oxygen polarity [14]. In this paper, we conduct further detailed analysis on the experimental results together with theoretical calculations in order to unveil the polarity selection mechanism, and finally find that the high pressure between $Mg_xZn_{1-x}O$ semiconductor alloy and MgO/Al_2O_3 substrate triggers the polarity alternation from Zn-polarity to O-polarity for thick MgO and ultrathin MgO, respectively. The ultrathin MgO layer was found to not only serve as the soft pad between the epilayer and substrate to interlink these two distinct structures, but also provides suitable pressure environments for the abrupt structural transformation from cubic into wurtzite phase inside the first few MgZnO layers. It is exactly the structural transformation that triggers the occurrence of O-polarity inside MgZnO comparing with Zn-polar MgZnO on a thick MgO template, and in the meantime accommodates the large lattice mismatch without introducing more dislocation defects. Lastly, the effect of high pressure on polarity selecting mechanism and the improved crystalline quality is partially demonstrated by the sensitive and superior photoresponse behaviour of photodetector devices in the ultraviolet spectrum region.

Atomic depositions were conducted by using radio-frequency plasma assisted MBE (rf-MBE) with highly purified material sources such as metal Zn (7N), metal Mg (5N) and atomic oxygen atoms in oxygen plasma with charged particles deflected. The structural evolution during the growth was monitored by *in situ* reflection high-energy electron diffraction (RHEED) and further characterized by using a high-resolution Cs-corrected scanning transmission electron microscope (STEM). Theoretical calculations were conducted by employing a strain relaxation model which has been extensively approved. The micron-size inter-digital metal–semiconductor–metal (MSM) Schottky diodes were fabricated based on the films by using Au-(40 nm)/Ti-(20 nm) as electrodes. Current–voltage (I–V) curves in the dark and under photon irradiation were measured by using a Keithley 6487 semiconductor parameter analyser. Different irradiation environments were provided by using a mercury lamp with a selectable wavelength of 365 nm and 254 nm and a SpectraPro-500i (Acton Research Corporation) optical system with a Xe-arc lamp combined with a monochromator as the light source, respectively. Custom designed Labview programs were used during the dark- and photo-electrical measurements. The power of the monochromatic UV light source was calibrated by comparing the counts of a standard power meter and those of the photomultiplier in the measurement system at the same wavelengths.

Corundum alumina has been reported to be a complicated oxide crystal with several different atomic surfaces in the (0 0 0 1) plane which can be prepared by different chemical and vacuum treatments [16]. Based on our previous vacuum treatment technique, we can obtain a uniform oxygen-terminated surface [17, 18], which was solidly approved by the clear observation of one oxygen interfacial monolayer between MgO and Al_2O_3 substrate [14]. This oxygen monolayer modifies the original Al and O co-latticed complex surface structure into a uniform one-atom-terminated surface and hence serves as a key epitaxial template for the determination of the following atomic stacking sequence along [0 0 0 1] direction. It greatly simplifies the varying experimental conditions and makes the following analysis much easier. On the uniform oxygen matrix, a MgO layer with different thickness was epitaxially deposited in an ordered alternation of Mg and O atoms, which significantly influenced the strain environment inside the MgZnO/MgO/Al_2O_3 system.

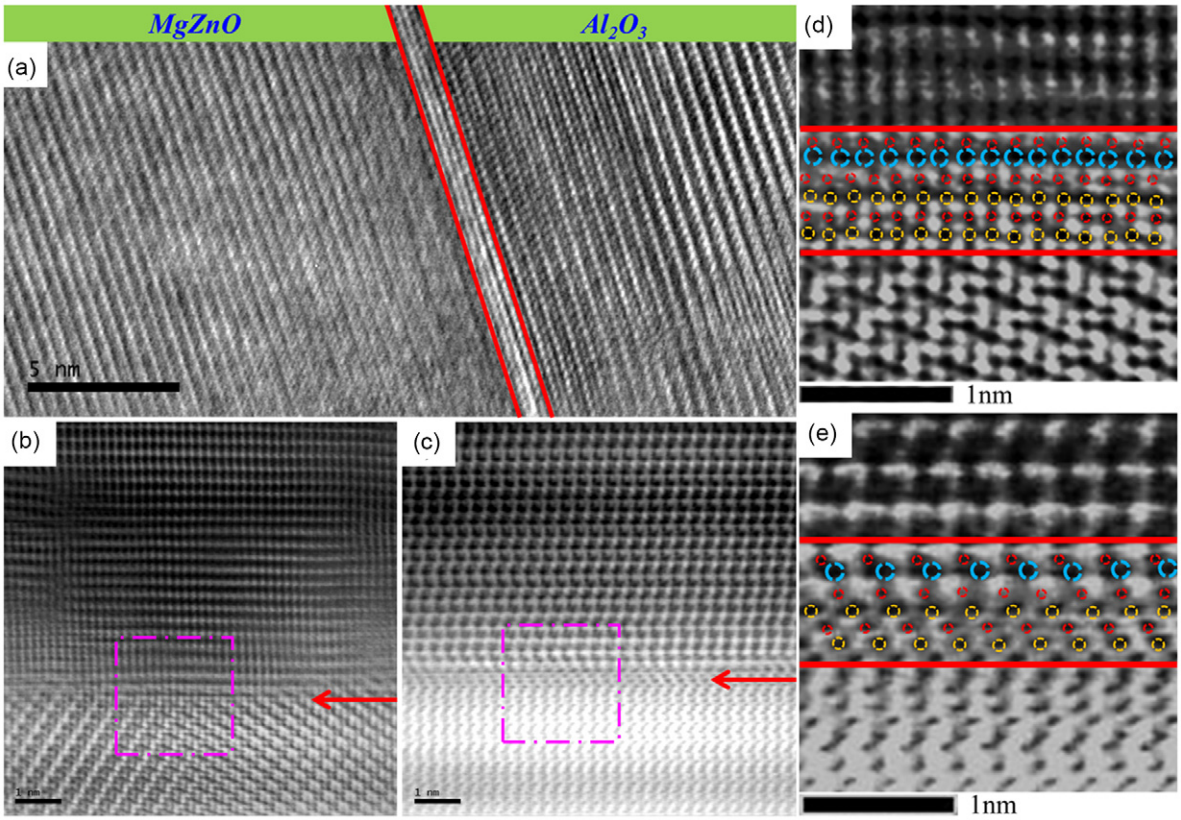

Figure 1. Atomic-resolution TEM image in (*a*) and STEM images in (*b*)–(*e*) of MgZnO(0 0 0 1)/ultrathin-MgO(1 1 1)/Al_2O_3(0 0 0 1), (*a*) shows the cross-section along directions of MgZnO ⟨1 0 −1 0⟩ in which the bright area is marked between red lines for MgO and structural transition layer of MgZnO; (*b*) and (*c*) show the magnified interfacial structure along MgZnO ⟨1 1 −2 0⟩ and ⟨1 0 −1 0⟩; the enlarged atomic configurations of the selected areas in figures 1(*b*) and (*c*) are shown in (*d*) and (*e*), respectively.

In this paper, high-quality MgO/Al_2O_3 samples were prepared by rf-MBE adopting a similar growth condition described in our previous work [18]. The atomic arrangements of the interfacial structure of MgZnO/MgO/Al_2O_3 are shown in high-resolution TEM and STEM images in figure 1, and the images along [1 0 −1 0] can also be found in our previous paper [14]. Figure 1(*a*) shows the structural evolution of MgZnO/MgO/Al_2O_3 and the bright region between two red lines is marked in order to elucidate the ultrathin MgO and nanometre-thick structural transforming region. Figures 1(*b*) and (*c*) show the magnified interfacial structure along MgZnO ⟨1 1 −2 0⟩ and ⟨1 0 −1 0⟩, besides the atomic configurations of the structural transforming areas which are labelled and shown in figures 1(*d*) and (*e*) respectively. The structural evolution suggests that oxygen termination was efficiently achieved and well-defined cubic MgO was deposited on the oxygen template. The rock-salt cubic nature of the MgO layer agrees well with the lowest energetic state of rock-salt structures in these theoretical investigations [11, 14, 15], and consequently, the explanation of polarity selection of $Mg_xZn_{1-x}O$ on MgO/Al_2O_3 based on wurtzite MgO becomes vulnerable. One purpose of this paper is to reveal the real relaxation mechanism occurring in this MgO layer when decreasing the thickness to nanometre scale.

The strain relaxation mechanism is proposed to explain the relaxation process of MgO grown on Al_2O_3 in this section, which was well approved by *in situ* RHEED monitoring results during the MBE epitaxial growth. Relaxation processes have been well studied in previous literatures on other material systems [19–21], and it has been widely recognized that the strained state is favourable until the energy of strained film exceeds a certain dislocation energy with the film thickness exceeding a critical value. In this paper, we adopt the same analysis route for this oxide system as that was successfully approved in GeSi alloy by considering their merits in dealing with large lattice-mismatched systems [21].

The areal strain energy density is

$$E_h = 2G\left(\frac{1+v}{1-v}\right)hf^2. \tag{1}$$

The energy density of screw dislocation bearing minimum energy is

$$E_D = \left(\frac{Gb^2}{8\pi\sqrt{2}a}\right)\ln\left(\frac{h}{b}\right), \tag{2}$$

where G, v, a, b, f donate film shear modulus, Poisson's ratio, lattice constant, magnitude of Burger's vector of MgO film, and lattice mismatch of MgO film and Al_2O_3 substrate, respectively.

For convenience, we use in this paper a critical thickness, H_c, which is determined by the equation of $2G((1+v)/(1-v))H_c f^2 = (Gb^2/8\pi\sqrt{2}a)\ln(H_c/b)$. We can get a critical thickness of 6.3 Å for unrelaxed strained rock-salt MgO film on alumina (0 0 0 1) substrate by considering

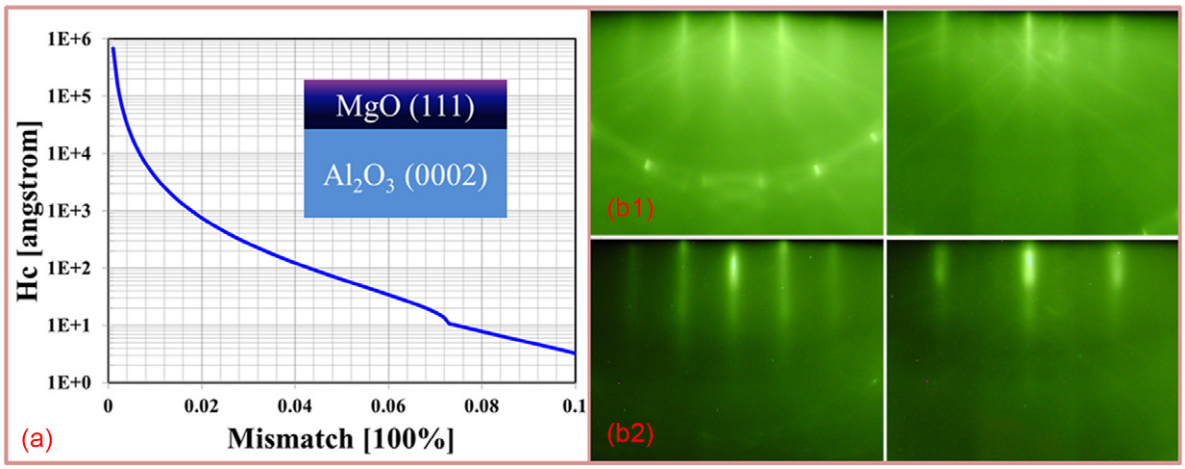

Figure 2. (*a*) Energetic calculation of critical film thickness of unrelaxed MgO with different lattice mismatch compared to substrates; (*b*) RHEED patterns recorded during the growth of MgO on Al_2O_3 substrate, transition is distinguished from (*b*1) highly strained cubic MgO (1 1 1) and (*b*2) relaxed MgO (1 1 1) on sapphire.

the mismatch of 8.5%. The calculation results are shown in figure 2(*a*). In this calculation, we adopted a lattice constant of 2.982 Å along [1 0 –1] and a Burger's vector of 4.216 Å along [1 0 0]. The above energetic result was consistent with our experimental estimation of ∼1 nm by RHEED observation and STEM characterization. In figure 2(*b*1), sharp and streaky RHEED patterns of the highly strained MgO ultrathin layer indicate the achievement of an atomic-flat surface, which was inherited from the alumina (0 0 0 1) substrate. The distinct transition features in RHEED patterns can be found in figure 2(*b*2). The obvious difference of horizontal distances between RHEED lines in figures 2(*b*1) and (*b*2) suggests that the MgO layer firstly held the lattice constant of alumina, in a highly strained state. If we increase the growth time and hence the thickness, by one/two-halves of that shown in figure 2(*b*1), it immediately transform into the intrinsically relaxed rock-salt structure with a bigger lattice constant. The secondary electron diffraction patterns of Al_2O_3 substrate plus the weak streaky lines superimposed on that of MgO in figure 2(*b*1) confirm the ultrathin thickness of the epitaxial MgO layer. While, the large spotty RHEED pattern on top of the streak lines indicates the relaxation process–growth mode transition from 2D planar growth to three-dimensional (3D) island growth in figure 2(*b*2). The thickness for MgO in figure 2(*b*1) could be estimated to be about 5 Å as confirmed in the inset of figures 1(*b*) and (*c*). The critical thickness from 7.5 to 10 Å determined from experimental data was consistent with the relaxation calculation results. On these strained and relaxed MgO surfaces, two distinct electric polarities of $Mg_xZn_{1-x}O$ with different crystalline quality can be reproducibly obtained via strain relaxation assisted structural transformation, which is discussed below.

Static pressure exerted on crystalline oxides can dramatically change materials' properties, especially crystal structures. It was reported that ZnO could transform from wurtzite (space group *P*63*mc*) to rock-salt cubic (space group *Fm*3*m*) structure when static compressive pressure is larger than 9.1 GPa [7, 10]. In this section, the planar strain existing inside the growth plane is also demonstrated to play an important role in alternating the crystal structure of $Mg_xZn_{1-x}O$ films grown on top of MgO templates. Epitaxial growth of wurtzite $Mg_xZn_{1-x}O$ on highly strained MgO/Al_2O_3 is completely different from that on relaxed MgO/Al_2O_3, because lattice mismatches (or strain states) are significantly distinguishable from each other, with values of 18.2% and 9% for unrelaxed and relaxed MgO, respectively. This big difference determines the phase transition mechanism, and consequently the polarity of epitaxial $Mg_xZn_{1-x}O$ layers. The STEM results in figure 1 suggest that the phase transition should be wurtzite-$Mg_xZn_{1-x}O$/cubic-$Mg_xZn_{1-x}O$/cubic-MgO/Al_2O_3 on highly strained cubic MgO, while wurtzite-$Mg_xZn_{1-x}O$/cubic-MgO/Al_2O_3 will be the result on a relaxed MgO template from our previous work and other literatures [11, 22], and consequently they possess different polarities of O-polar and Zn-polar, respectively. We can observe the sequential evolutions from *in situ* electron diffraction patterns. In figure 3, column (*a*) shows the diffraction change from strained MgO $\langle 1\,1\,-\,2\rangle$ to $Mg_xZn_{1-x}O\langle 1\,0\,-\,1\,0\rangle$ buffer layer. We cannot recognize any structural transition along this direction. However, distinguishable differences were observed in the direction of MgO $\langle 1\,-\,1\,0\rangle$. At the beginning of deposition of $Mg_xZn_{1-x}O$, a highly twisted transient diffraction pattern appears in figure 3(*b*2). Afterwards, a streaky electron diffraction pattern indicating 2D growth mode and structural relaxation from cubic into wurtzite $Mg_xZn_{1-x}O$ is shown in figure 3(*b*3). The growth mode dominated the following growth of $Mg_xZn_{1-x}O$ layers. For clarification, the simulation result of electron diffraction along the rock-salt [1 –1 0] and wurtzite [1 1 –2 0] directions are illustrated in figure 3(*c*), which was processed with the help of Electron Diffraction Simulation in the 'Web Electron Microscopy Applications Software' package [23]. The identical characteristics suggest that the twin-crystal cubic nature of the structure existed in the initial growth of the MgZnO layer, as shown in figure 3(*b*2).

The above structural evolution can be confirmed by the atomic-resolution STEM results in figure 4. The upper panels

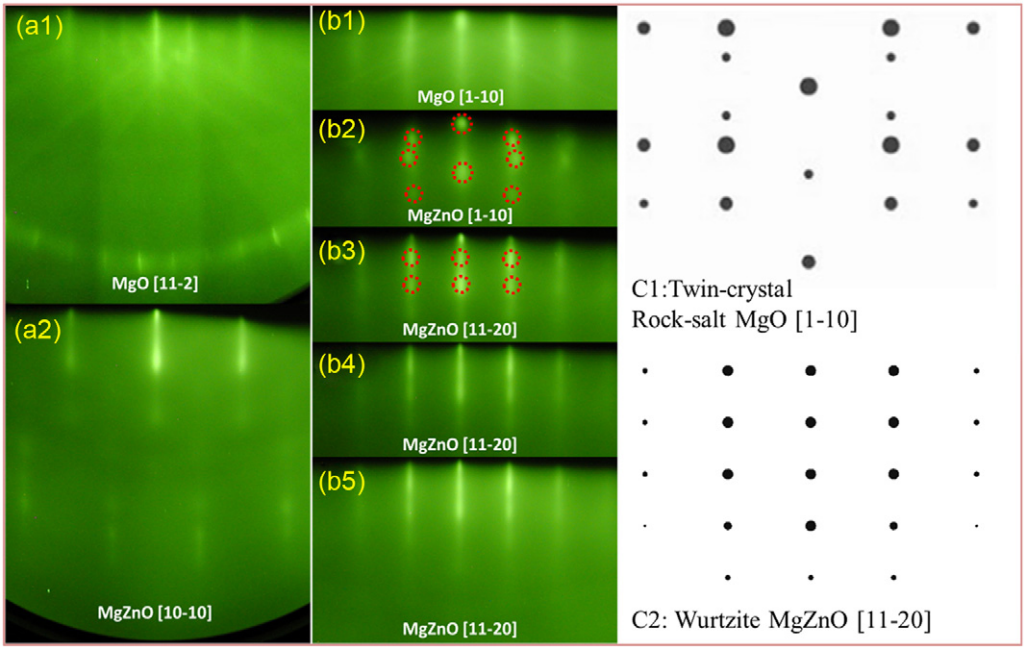

Figure 3. The structure evolution around the MgZnO/MgO interface; (*a*)-(*b*) RHEED patterns along two independent directions marked inside diffraction patterns, (*c*) simulated electron diffraction pattern for rock-salt cubic structure along [1 −1 0] and wurtzite along [1 1 −2 0] directions in (*c*1) and (*c*2) respectively.

(*a*1) and (*a*2) show the enlarged cross-section image from the selected regions in figure 1 inside the pink squares. The atoms are labelled by broken circles with different colours. Al double atomic layers (violet circles) and zigzag O–Al–O structures (red circles for oxygen) can be observed easily, which also served as the signatures for identifying the atomic stacking above. MgO (yellow circles for Mg) is revealed to bear a uniform two-layer structure and provide the unrelaxed template for unipolar epilayers. MgZnO layers are identified by the big Mg_xZn_{1-x} atoms. The relative position inside MgZnO were determined by bright interstitial space 1 and 2 marked in figures 4(*b*1) and (*b*2). We also summarize the atomic evolutions in the centre panel of figure 4. Strained MgO template (S.T.), cubic Mg_xZn_{1-x} layer (first structural transition layer, T1), wurtzite oxygen layer (second structural transition layer, T2) and above polar MgZnO layer (P.L.) are clearly labelled in this cross-view atomic model. Besides, the transition layers are also partly labelled on the above panel for clarity. The STEM results suggest that only one $Mg_xZn_{1-x}O$ monolayer inherited a six-fold cubic structure and structural change from six-fold cubic to four-fold wurtzite occurred abruptly in the second oxygen layer, and finally, resulted in oxygen polarity in $Mg_xZn_{1-x}O$ films on the highly strained MgO template. On the contrary, we did not observe analogue structural evolution in wurtzite-$Mg_xZn_{1-x}O$/relaxed-MgO, which agrees with abrupt structural change from six-fold cubic to four-fold wurtzite during the growth of $Mg_xZn_{1-x}O$ in a previous report [11]. In order to elucidate the special structural relaxation mechanism clearly, we need to figure out in which condition the structure of MgZnO changes into metastable cubic structures under planar strain inside the growth plane, which serves as the central issue to determine the polarity. Detailed strain analysis is listed as follows.

In the case of ultrathin MgO, the mismatch of ZnO and MgO is $\varepsilon_{\text{total}} = 118.2\% \times \varepsilon_{\text{MgZnO}} + \varepsilon_{\text{MgO}} = 18.2\%$ and then the pressure inside the films is

$$P_{\text{MgO}} = P_{\text{Mg}_{\text{ZnO}}} = Y \times \varepsilon. \tag{3}$$

Finally, by applying the parameters in table 1 to equation (3), we can get the pressure between the MgZnO epilayer and the MgO template as 13.7 GPa with strain inside the films being 11.5% and 4.6% respectively for MgZnO and MgO. Calculation results are consistent with the lattice increase of about 5% in MgO extracted from figure 4, but much larger than the lattice decrease in the MgZnO layer which is about 6%. This 'inconsistency' can be reasonably explained by gradual relaxation under the influence of the above MgZnO layers. While in the case of relaxed MgO, mismatch between MgO and MgZnO is much smaller with a value of 9%. We can get the stress between two oxides as 6.8 GPa with a lattice change of MgZnO inside (0 0 0 2) plane as 5.7%. Considering that the Poisson ratio of wurtzite MgZnO is similar to that of ZnO of 0.351 and cubic MgZnO to that of MgO of 0.186, the volume ratio (V/Vo: V and Vo are volume with and without pressure) would be 82% and 94% for the MgZnO films grown on strained and relaxed MgO, respectively. The volume variation under static compressive pressure is shown in figure 4(*c*) with blue lines by using the relation from [10]. Two markers with red and green colour in figure 4(*c*) indicate the volume ratios and in-plane pressures of the strained and relaxed MgO buffer. The red colour is designated in order to show the pressure-induced phase transition from wurtzite to cubic structure inside MgZnO. Therefore, we can conclude that nanoscale phase transition of MgZnO will happen under in-plane stress between 6.8 and 13.7 GPa, which occurs in the same range under 3D compressive pressure.

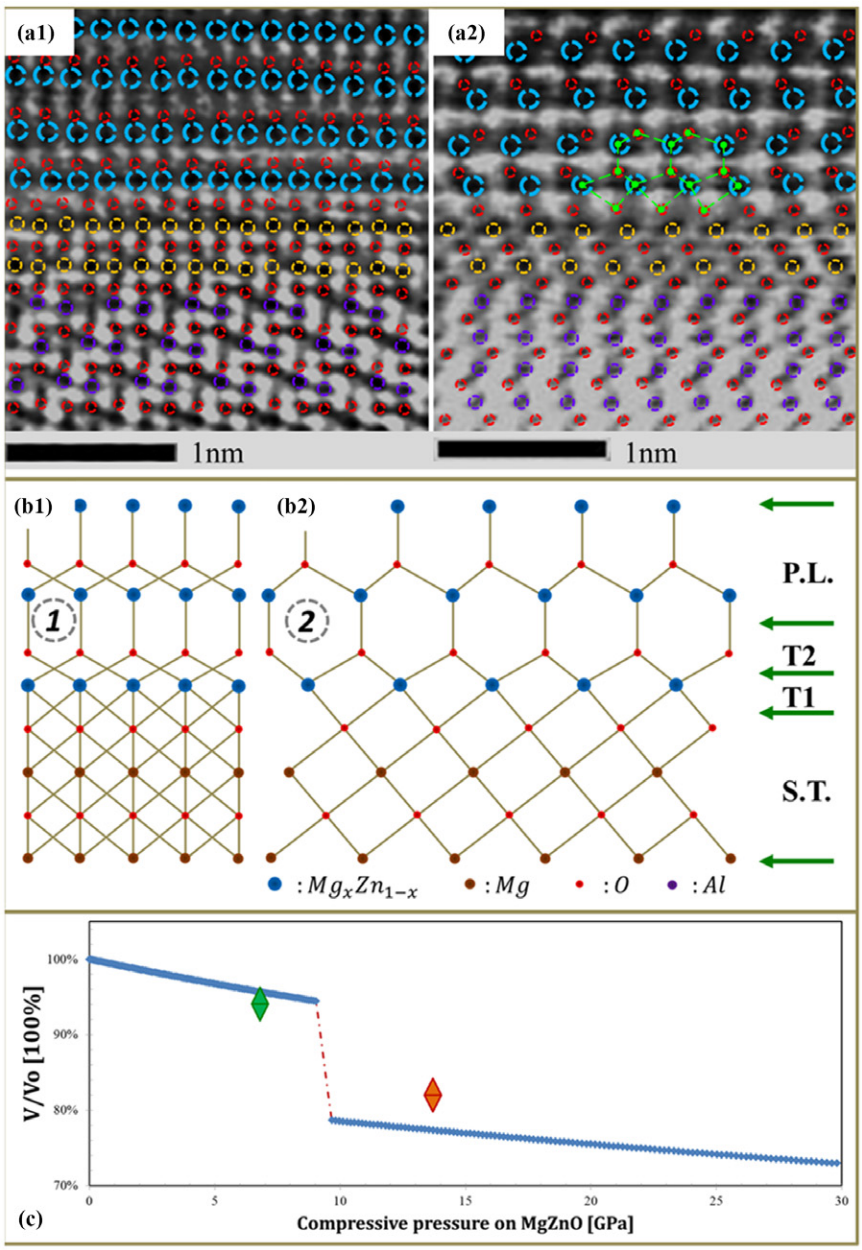

Figure 4. (a1) and (a2) show the magnified high-resolution STEM images in both directions selected from the pink squares of figure 1; (b1) and (b2) show the respective stick and ball models along MgZnO $\langle 1\,1\,-2\,0\rangle$ and $\langle 1\,0\,-1\,0\rangle$ for the above panel, in which different layers are labelled on the right; (c) shows the calculated volume ratio for $Mg_xZn_{1-x}O$ at different compressive presses (Note: the blue line demonstrating the transition for ZnO is shown here for comparison).

By comparing the crystalline quality of MgZnO on strained and relaxed MgO buffers, a strained buffer was found to serve as a better candidate to accommodate the large lattice mismatch between sapphire and the MgZnO epilayer, consequently suppressing the defects on the above MgZnO epitaxial layer a lot. Detailed analysis on the crystalline quality and defect analysis will be presented elsewhere. In this section, we would like to qualify the crystalline quality by simply studying the electric response of the film under photo irradiation. Based on the film $Mg_{0.5}Zn_{0.5}O$-(200 nm)/$Mg_{0.2}Zn_{0.8}O$-(20 nm)/MgO-(0.5 nm)/Al_2O_3 synthesized by rf-MBE employing a 'quasi-homo buffer' technique [18, 24], we fabricated 5-by-5 μm MSM inter-digital double Schottky diode by using photo-lithography. Au-(40 nm)/Ti-(20 nm) metal films are patterned as electrodes with 5 μm width for both gap and finger, and with 300 μm length of finger. The magnified active photoresponse region is shown in the lower inset of figure 5. I–V characteristics under different irradiation conditions are shown in the top inset of figure 5. Current in dark environment or under irradiation of 365 nm photon is less than 0.1 nA, which suggests a large Schottky barrier height (SBH) between the Ti/Au electrode and the $Mg_{0.5}Zn_{0.5}O$ epilayer [25]. With a high Schottky barrier, the dark current can be well suppressed, and the rejection ratio can be promisingly high, as shown below. The current under 254 nm irradiation is several orders

Table 1. Lattice parameters and mechanical properties[1] of sapphire, MgO and ZnO.

	Lattice constant			Misfit of c	Shear modulus (G)	Yang's modulus (Y)
Al_2O_3	4.759 Å [1 1 −2 0]	8.242 Å [1 0 −1 0]	12.99 Å [0 0 0 1]	0	156.5 GPa	395.8 GPa (NIST-data)
MgO	4.216 Å [1 0 0] 2.982 Å [1 0 −1]	— 5.164 Å [1 1 −2]	7.302 Å [1 1 1]	8.5% (refer to Al_2O_3)	124.3 GPa	294.7 GPa (NIST-data)
ZnO	3.249 Å [1 1 −2 0]	5.627 Å [1 0 −1 0]	5.205 Å [0 0 0 1]	18.2% (refer to Al_2O_3) 9% (refer to MgO)	44 GPa	119 GPa (NIST-data)

Note: The misfit of MgO and ZnO with Al_2O_3 is the misfit of rotated lattice. Because of the structural similarity between wurtzite MgZnO and ZnO, we adopted ZnO crystal lattice parameters for that of MgZnO in the calculations.

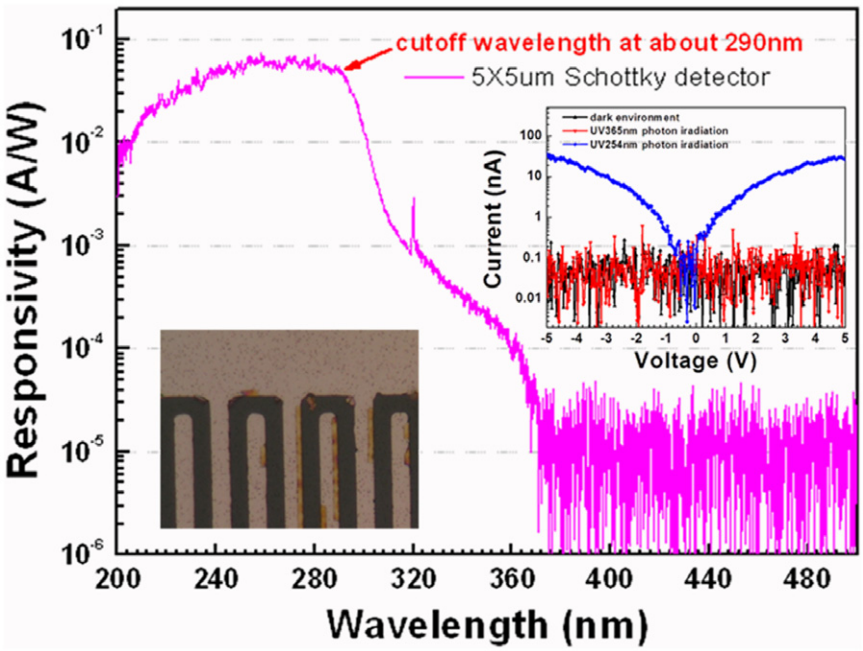

Figure 5. Photoresponsibility of MSM double Schottky diode in visible to ultraviolet spectrum range; inset below shows the microscopic image of the active area with 5-by-5 μm inter-digital electrodes; inset above shows the I–V curves of the Schottky diode under different irradiation conditions.

of magnitude larger than that in the dark. Besides, the symmetrical I–V curve demonstrates characteristics of back-to-back Schottky barriers inside the Schottky diode and a reduced Schottky barrier model must be adopted to explain the gain mechanism [25, 26]. A large external quantum efficiency of 23% can be extracted from the photoresponse of 53 mA W^{-1} at a wavelength of 289 nm. More than four orders of rejection ratio of ultraviolet (wavelength from 240 to 290 nm) to visible light photoresponse and the sharp response edges confirm the crystalline quality of the MgZnO film grown on a strained-MgO/sapphire template. The photoresponse in 290–370 nm wavelength range is caused by photo-induced electrons inside the lower-Mg-content buffer, which can also be seen in the absorption spectra [18].

[1] The mechanical parameters are from materials with the least fraction of porosity which are published by National Institute of Standards and Technology.

In this paper, we proposed a theoretical route for investigating the structure evolution of MgO grown on large lattice-mismatched substrate, which is approved by our experimental analysis including *in situ* RHEED monitoring and *ex situ* TEM results. Dislocation related strain relaxation was suggested to happen around 1 nm thick MgO on Al_2O_3, which has a strained cubic structure instead of a wurtzite phase. Based on the fact of strain-environment dissimilarity of MgZnO/strained-MgO and MgZnO/relaxed-MgO, we clarified that lattice pressure-induced nanoscale structural transformation in the first two layers of MgZnO triggered the polarity flipping on the ultrathin MgO comparing with the case on thick relaxed MgO template. Finally, back-to-back MSM Schottky photodetectors fabricated based on the films and photoresponse performances demonstrated the superior ability of nanoscale structural transformation for accommodating the large lattice mismatch and promoting the crystal qualities.

Acknowledgments

This work is supported by the Ministry of Science and Technology (Grant nos 2011CB302002, 2011CB302006, 2009CB929404) of China, the National Science Foundation (Grant nos 61076007, 11174348, 51272280, 11274366, 61204067), and Chinese Academy of Sciences. The author would like to thank Dr Bo Li for valuable discussions and encouragement during the preparation of this work.

References

[1] Karrer U, Ambacher O and Stutzmann M 2000 *Appl. Phys. Lett.* **77** 2012
[2] Wang Z L and Song J H 2006 *Science* **312** 242
[3] Yakimova R, Selegard L, Khranovskyy V, Pearce R, Lloyd Spetz A and Uvdal K 2012 *Front. Biosci.* **4** 254
[4] Tsukazaki A, Ohtomo A, Kita T, Ohno Y, Ohno H and Kawasaki M 2007 *Science* **315** 1388
[5] Huang D, Visconti P, Jones K, Reshchikov M, Yun F, Baski A, King T and Morkoc H 2001 *Appl. Phys. Lett.* **78** 4145
[6] Mei Z X, Du X L, Wang Y, Ying M J, Zeng Z Q, Zheng H, Jia J F, Xue Q K and Zhang Z 2005 *Appl. Phys. Lett.* **86** 112111
[7] Bates C, White W and Roy R 1962 *Science* **137** 993
[8] Hor P H *et al* 1987 *Phys. Rev. Lett.* **58** 911
[9] Iwasa Y *et al* 1994 *Science* **264** 1570
[10] Desgreniers S 1998 *Phys. Rev.* B **58** 14102
[11] Kato H, Miyamoto K, Sano M and Yao T 2004 *Appl. Phys. Lett.* **84** 4562
[12] Martinez-Boubeta C, Botana A, Pardo V, Baldomir D, Antony A, Bertomeu J, Rebled J, Lopez-Conesa L, Estrade S and Peiro F 2012 *Phys. Rev.* B **86** 041407
[13] Schleife A, Fuchs F, Furthmüller J and Bechstedt F 2006 *Phys. Rev.* B **73** 245212
[14] He X, Gu L, Guo S, Liu Z L, Yu R, Mei Z X, Du X L, Liu B, Ikuhara Y and Duan X 2013 *J. Phys. D: Appl. Phys.* **46** 145303
[15] Zhu Y Z, Chen G D, Ye H, Walsh A, Moon C Y and Wei S H 2008 *Phys. Rev.* B **77** 245209
[16] Eng P J, Trainor T, Brown G Jr, Waychunas G, Newville M, Sutton S and Rivers M 2000 *Science* **288** 1029
[17] Mei Z X, Wang Y, Du X L, Ying M J, Zeng Z Q, Zheng H, Jia J F, Xue Q K and Zhang Z J 2004 *Appl. Phys.* **96** 7108
[18] Liu Z L, Mei Z X, Zhang T C, Liu Y P, Guo Y, Du X L, Hallen A, Zhu J J and Kuznetsov A Yu 2009 *J. Cryst. Growth* **311** 4356–9
[19] Van Der Merwe J H 1963 *J. Appl. Phys.* **34** 123
[20] Matthews J W, Mader S and Light T B 1970 *J. Appl. Phys.* **41** 3800
[21] People R and Bean J C 1985 *Appl. Phys. Lett.* **47** 322
[22] Yuan H T, Liu Y Z, Mei Z X, Zeng Z Q, Guo Y, Du X L, Jia J F, Zhang Z and Xue Q K 2010 *J. Cryst. Growth* **312** 263
[23] Zuo J M and Mabon J C 2004 Web-based Electron Microscopy Application Software: Web-EMAPS *Microsc. Microanal.* **10** (suppl. 2) 1000 http://emaps.mrl.uiuc.edu/
[24] Du X L, Mei Z X, Liu Z L, Guo Y, Zhang T C, Hou Y N, Zhang Z, Xue Q K and Kuznetsov A Yu 2009 *Adv. Mater.* **21** 4625
[25] Hou Y N, Mei Z X, Liu Z L, Zhang T C and Du X L 2011 *Appl. Phys. Lett.* **98** 103506
[26] Katz O, Garber V, Meyler B, Bahir G and Salzman J 2001 *Appl. Phys. Lett.* **79** 1417